Article

An Attempt to Design Thermosalient Crystals by Co-Crystallization: The Twisted Angle between Aromatic Rings

Xingchen Hu [1], Yuntian Xiao [1], Luguang Qi [1], Yunhe Bai [1], Ying Sun [1], Yang Ye [1] and Chuang Xie [1,2,3,*]

1   School of Chemical Engineering and Technology, Tianjin University, Tianjin 300072, China; xingchenhu@tju.edu.cn (X.H.); xyt96@tju.edu.cn (Y.X.); qiluguang@tju.edu.cn (L.Q.); yunhe_bai@tju.edu.cn (Y.B.); sy7998@tju.edu.cn (Y.S.); yeyang96@tju.edu.cn (Y.Y.)
2   National Engineering Research Center of Industrial Crystallization Technology, Tianjin University, Tianjin 300072, China
3   State Key Laboratory of Chemical Engineering, Tianjin University, Tianjin 300072, China
*   Correspondence: acxie@tju.edu.cn

Abstract: Thermosalient (TS) crystals have gained considerable attention due to their potential applications in various fields, including in actuators, sensors, energy harvesting, and artificial muscles. Herein, co-crystallization was employed to construct TS crystals by forming a twisted angle between aromatic rings. Two multicomponent trimethoprim (TMP) TS cocrystals, TMP-25HBA and TMP-OA, were obtained. Differential scanning calorimetry (DSC) and variable-temperature powder X-ray diffraction (VT-PXRD) revealed that TMP-OA undergoes a solid-to-solid phase transition, while TMP-25HBA does not exhibit any phase transition. To the best of our knowledge, TMP-25HBA is the first multicomponent TS crystal without phase transition. The TS effect of both crystals is a result of the unit cell's anisotropic expansion.

Keywords: thermosalient crystals; jumping cocrystals; twisted angle; mechanical properties

1. Introduction

The mechanical response of molecular crystals under light or heat stimulation, known as the salient effect [1–3], has gained much attention from researchers due to its potential in various fields, including sensors, actuators, artificial muscles, and energy harvesting [4–7]. Dr. Chizhick et al. [8] reviewed the mechanical response molecular crystals before 2015 in detail, and their research has made outstanding contributions to this field of photomechanical molecular crystals. The 4-hydroxy-2-(2-pyridyl methylene) hydrazide photomechanical crystal [9] reported by Dr. Chizhick et al. is the highest recorded deformation of low-temperature bending crystals.
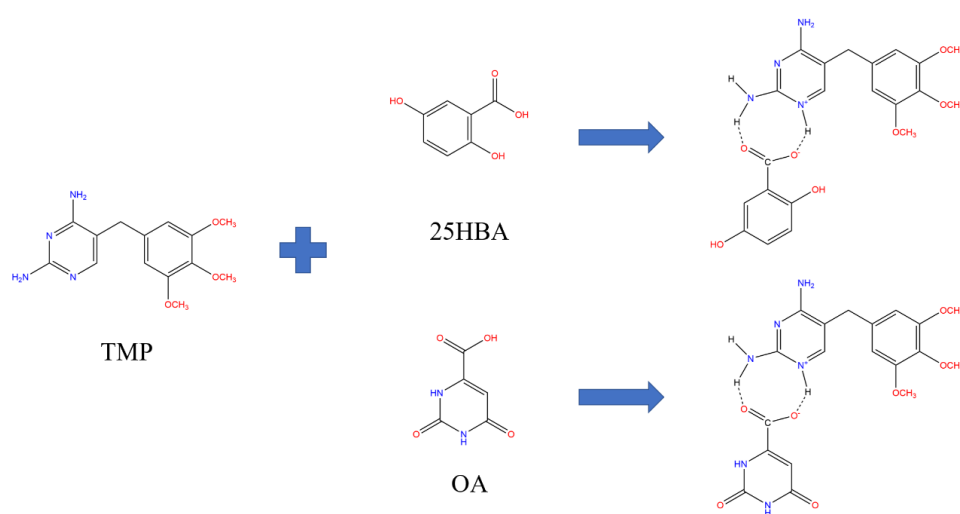
Among the different types of mechanical response crystals, thermosalient (TS) crystals, or jumping crystals, have gained considerable interest due to their ability to convert thermal energy into mechanical energy during heating or cooling [10–14]. Currently, there are less than 50 cases of jumping crystals documented in the past four decades [1,8,15,16].

To construct TS crystals, it is necessary to comprehend their temperature response mechanism. Current research suggests that the anisotropic change of the unit cell induced by the change in molecular conformation or packing during heating or cooling results in the crystal's anisotropic stress and causes crystal jumping [17]. This process is typically accompanied by the solid phase transformation of crystals, such as 1,4-diazabicyclo[2.2.2]octane [18], triphenylethenyl gold 4- chlorophenyl isocyanide complex [19], double ester naphthalene-2,3-diyl-bis(4-fluorobenzoate) terephthalic acid [20], 1,2,4,5-tetrabromobenzene [21], ox-itropium bromide [22], etc. In addition to the molecule conformation or packing changes during phase transition, desolvation can also induce crystal jumping, such as spironolactone–saccharin cocrystal [15], tetra-[2,3]thienylene tetracarboxylic acid [23], and pyrene tweezers [24]. However, there are five instances of crystal jumping without undergoing phase

transition [17,25–28], which all were found to have twisted angles between aromatic rings (Figure S1). However, it is extremely difficult to synthesize molecules with such unusual structures and crystallize them.

To address this challenge, a co-crystallization strategy in crystal engineering was employed to link molecules with weak connections to create a twisted angle between aromatic rings.

Trimethoprim (TMP), a typically used antibiotic containing benzene and pyrimidine rings, was used as the model substance. This study focused on the co-crystallization of TMP with 2,5-dihydroxybenzoic acid (25HBA) and orotic acid (OA) as additional components (Scheme 1), which both have a carboxyl group and an aromatic ring. The feasibility of this strategy was confirmed by the observation of the TS effect in both multicomponent crystals. The TMP-25HBA crystal is the first multicomponent TS crystal without phase transition reported to date. The results of this work may provide valuable reference for the design of TS crystals.

Scheme 1. Design of twisted conformations containing an aromatic ring via hydrogen-bonding interactions.

2. Experimental Part

2.1. Single Crystal Preparation

Preparation of TMP-2,5HBA: 87 mg of TMP and 46.2 mg of 25HBA were added into a glass bottle containing 5 mL of methanol solution. After dissolution, the solution was filtered with a 0.45 μm nylon filter membrane. The filtrate was placed in a clean glass vial and slowly volatilized at room temperature for 7–10 days to obtain the crystal of TMP-25HBA.

Preparation of TMP-OA: 87 mg of TMP and 46.8 mg of OA were added into a glass bottle filled with 10 mL of water. The glass bottle was heated to 75 °C to dissolve the solids. After the solid was completely dissolved, the solution was filtered with a 0.45 μm nylon filter membrane and added into a clean vial. The vial was then cooled to 25 °C at a rate of 0.05 °C/min to obtained crystal of TMP-OA.

2.2. Characterization

Hot-stage microscopic measurements were performed with a Linkam system, including a temperature-controlled stage LNP94/2 mounted on a microscope CX40P. TGA analysis was performed on a Mettler TGA/DSC 1 system (STARe, Mettler, Zurich, Switzerland). DSC was performed on a Mettler DSC 1 system (STARe, Mettler, Zurich, Switzerland). SCXRD measurement was conducted on a Rigaku Saturn 70 CCD diffractometer using Mo Kα radiation (λ = 0.71073 Å) with a graphite monochromator. Variable temperature powder X-ray diffraction data for TMP-OA were obtained on D8 advance (Bruck,

Hersbruck, Germany). Unit cell parameters for TMP-25HBA are obtained on D8 Venture (Bruck, Germany).

2.3. Theoretical Calculation

The Hirshfeld surface analysis of crystals was performed using CrystalExplorer21 [29] and the proportion of intermolecular contacts was quantified. The calculation of energy frameworks is also carried out by crystalExplorer21. Unit cell parameters at high temperature were obtained by Rietveld refinement by JADE 6 for VT-PXRD.

3. Results and Discussion

3.1. Observing TS Effect

The TS effect of TMP-25HBA and TMP-OA crystals was observed using HSM (Figure 1). For TMP-25HBA, the temperature range for crystal jumping was relatively wide. Crystal movement (Movie S1) was observed at 180 °C and it jumped out of view (Figure 1a) at 183 °C. Breakage during jumping occurred when being heated to 200 °C. Such a TS effect was not observed during the cooling process. In contrast, for TMP-OA, we monitored the TS effect during both heating and cooling processes (Figure 1b). Crystal movement was observable during all temperature cycles (Movies S2–S5). We also discovered that TMP-OA had the highest reported crystal temperature with the maximum TS effect (260 °C). In addition, TMP-OA kept bright before and after the heating jump, indicating that its single crystal structure was well maintained during the jumping.
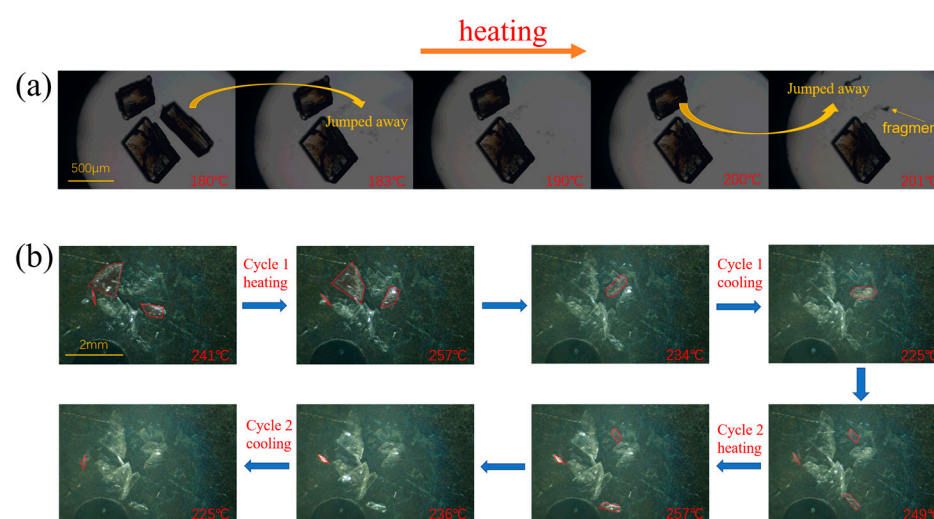

Figure 1. (**a**) Heating jump of TMP-25HBA (TMP: Trimethoprim; 25HBA: 2,5-dihydroxybenzoic acid) with heating rate of 10 °C/min monitored using the microscope; (**b**) thermal stimulation of TMP-OA (TMP: Trimethoprim; OA: Orotic acid) under two heating–cooling cycles between 190 °C and 265 °C.

3.2. Differential Scanning Calorimetry and Thermogravimetric Analysis

To gain a deeper understanding of the TS phenomena, single crystals of TMP-25HBA and TMP-OA were observed using differential scanning calorimetry (DSC) and thermogravimetric analysis (TGA). For the TMP-25HBA single crystal, the DSC curve contains numerous small endothermic peaks in the temperature range of 125–210 °C during heating (Figure 2a), indicating the presence of the TS effect [18–20,30,31], which is related to the crystal size distribution of the samples. No jagged DSC curve was collected for powdered samples of TMP-25HBA crystals within this temperature range. The reason might be that crystals of different sizes have different heat absorption conditions, and the heat transfer rates at different crystal planes varied. The thermogravimetric analysis of the TMP-25HBA crystal presents clearly uneven weight loss steps, while the TGA curve of TMP-25HBA powders is smooth (Figure 2c). The sudden weightlessness of TMP-25HBA crystals before decomposition temperature is likely due to some of the crystals jumping out of the crucible.

This could also be verified by the ash content of TMP-25HBA crystals being apparently less than that of the powders.
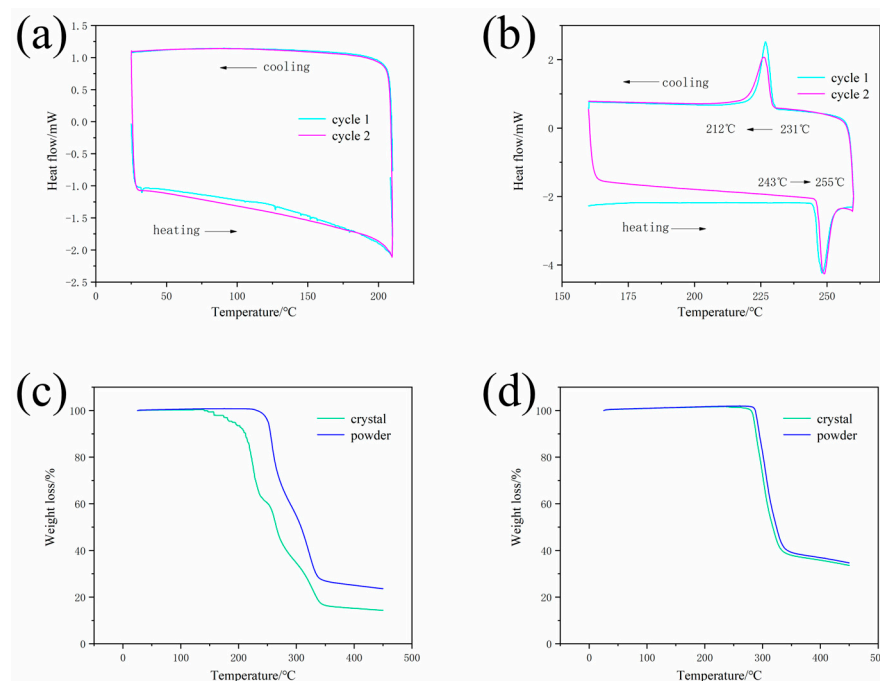

Figure 2. DSC curves of TMP-25HBA (**a**) and TMP-OA (**b**) on two heating–cooling cycles and TGA (Thermogravimetry Analysis) curves of TMP-25HBA (**c**) and TMP-OA (**d**). The heating and cooling rates are 5 °C/min.

In contrast, for TMP-OA, an endothermic peak between 243–255 °C and an exothermic peak between 231–212 °C were recorded during the first temperature cycle (Figure 2b), suggesting that the crystal could undergo phase transformation in this temperature range. The crystal form stable at low temperatures was named TMP-OA^{LT}, while the crystal form stable at high temperatures was named TMP-OA^{HT}. Such two-phase transition repeated during the second temperature cycle and the transition temperature range was consistent with cycle 1. The TS effect of TMP-OA was observed during the transition between these two phases, but the endothermic peak on the DSC curve did not have any sawtooth patterns. The TGA curves of TMP-OA crystal and powder were nearly identical (Figure 2d), indicating that it was difficult for TMP-OA crystals to escape the crucible during the heating process. The weak TS behavior of TMP-OA may be due to the flaky morphology, in addition to its crystal structure.

3.3. Variable-Temperature Powder X-ray Diffraction (VT-PXRD)

Variable-temperature powder X-ray diffraction (VT-PXRD) was employed to monitor any phase transformation of TMP-OA during the heating process. The temperature was raised to 265 °C and then cooled to 25 °C at the heating/cooling rate of 10 °C/min. X-ray diffraction information was collected at specific temperatures. At the same time, the VT-PXRD analysis of TMP-25HBA is also carried out, in order to further study whether there is a phase transformation during the heating process.

For TMP-25HBA, the phase stability of TMP-25HBA was confirmed by the fact that the number of diffraction peaks did not decrease or increase during the heating process (Figure 3a). In the range of 20.0°–22.0° (Figure 3b), the diffraction peak on the left side moves to a lower 2θ angle with the increase of temperature, and the position of the diffraction peak on the right side does not change. In the range of 44.0°–44.5° (Figure 3c), both diffraction peaks move to a lower 2θ angle. All these indicate that the unit cell of TMP-25HBA has anisotropic expansion or contraction.
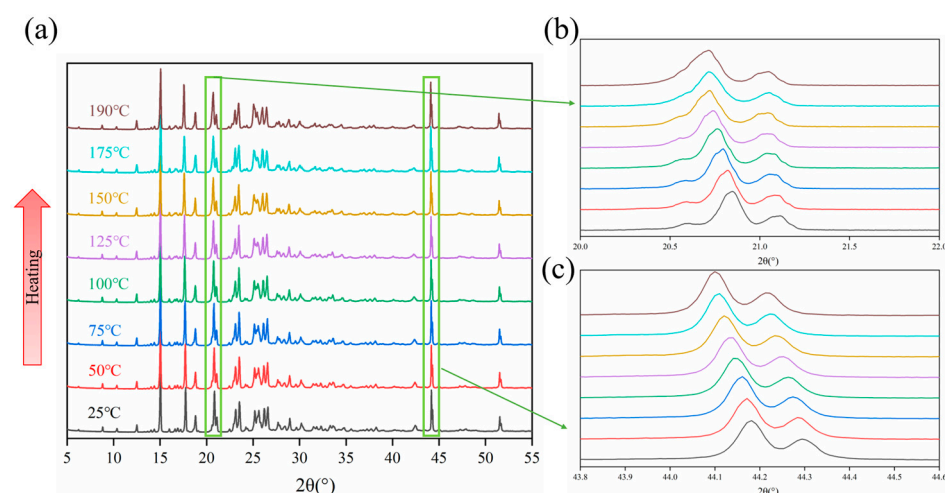
Figure 3. (**a**) VT-PXRD (Variable-temperature powder X-ray diffraction) patterns of TMP-25HBA during heating from 25 °C to 190 °C. (**b**) The PXRD peak shift of near 21.0°. (**c**) The PXRD peak shift of near 44.2°.

For TMP-OA, the variation of X-ray diffraction peak positions with temperature was carefully evaluated. Figure 4b showed that the diffraction peaks between 25° and 27.5° changed significantly as the temperature increased. As the temperature reached 265 °C, a new diffraction peak appeared between the two previously observed peaks, which shrunk during heating. This indicates a phase transition process that is also monitored by the DSC curve. The position of the diffraction peak in Figure 4c shifted to a lower 2θ angle during heating and then returned to its original position when being cooled. The peak shift is a sign of lattice expansion or contraction, depending on the hkl index. The reversible peak shift indicates reversible lattice expansion or contraction of TMP-OA.
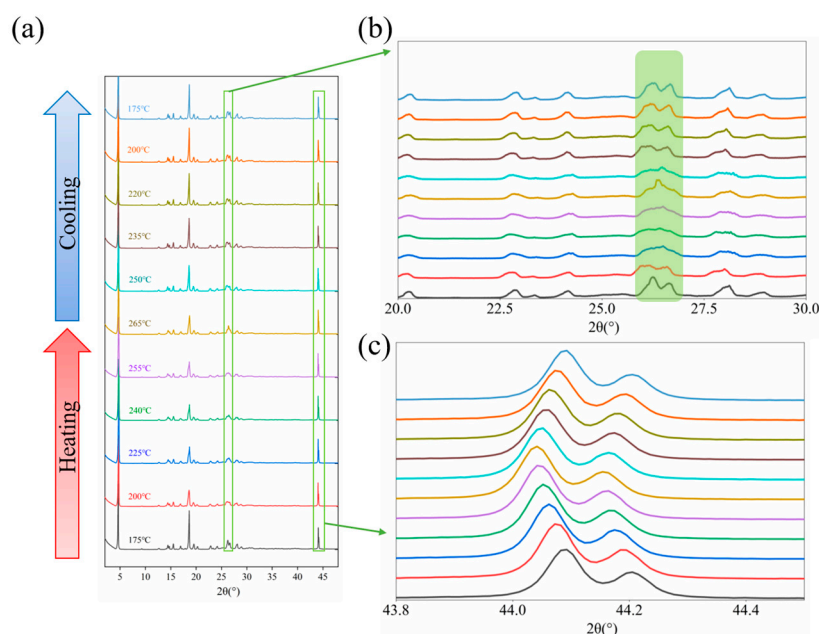

Figure 4. (**a**) VT-PXRD patterns of TMP-OA during heating/cooling from 175 °C to 265 °C. (**b**) Local magnification of X-ray diffraction peaks in the 2θ range of 20°~30°. (**c**) The PXRD peak shift of near 44.1°.

3.4. Thermal Expansion Coefficients

Temperature-dependent single-crystal structural analyses of TMP-25HBA were conducted to understand the mechanism underlying this thermo-responsive crystal jumping. Single crystal unit cell data were collected from 110 °C to 210 °C at a heating rate of

10 °C/min. Figure 5 shows the changes in the length of crystallographic a, b, and c axes of the single crystals of TMP-25HBA upon temperature changes, and the expansivity indicatrices of TMP-25HBA.
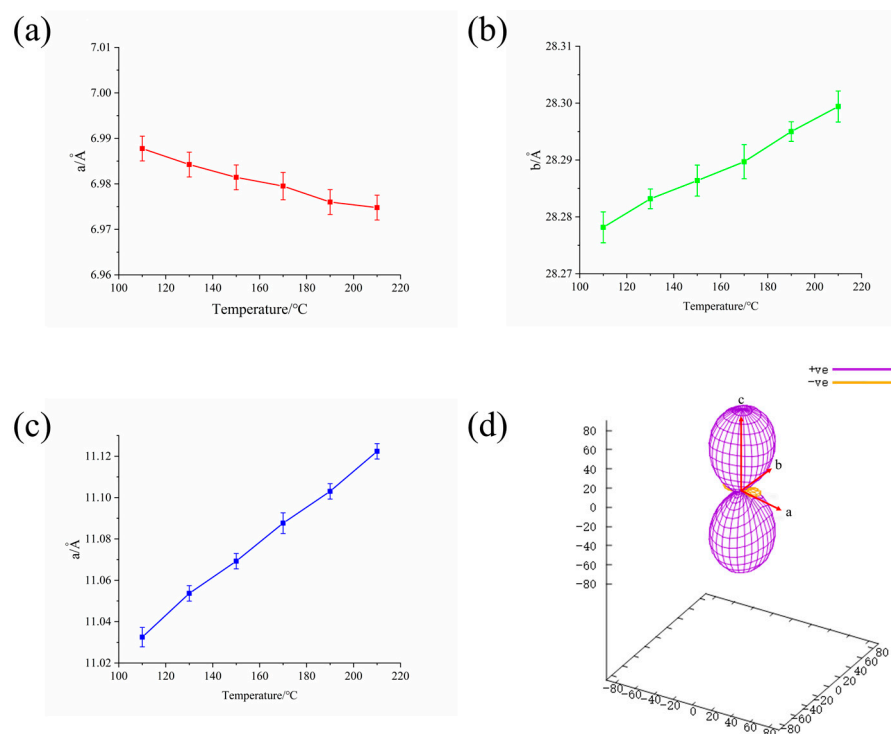

Figure 5. Temperature-dependent crystallographic parameters a (**a**), b (**b**) and c (**c**) axes and the expansivity indicatrices (**d**) of TMP-25HBA; purple and yellow represent positive and negative thermal expansion, respectively.

The unit cell of the TMP-25HBA crystal showed temperature-dependent anisotropic expansion/contraction which is considered a characteristic of jumping crystals. The selective anisotropic expansion of the unit cell occurred most obviously along the c-axis direction of C-H···π stacking between TMP molecules (Figure 6c). The unit cell contracted along the a-axis of the hetero-tetramer chain (Figure 6b). The length of the c-axis increased by 0.82% and the length of the a-axis decreased by 0.19% during heating from 110 °C to 210 °C. The lengths of axes a, b, and c are observed to have a linear relationship with temperature.

For TMP-25HBA, a special hetero-tetramer (Figure 6a) including two TMP molecules and two 25HBA molecules arrange in chains along the a-axis via the hydrogen bond interaction between 25HBA molecules (the red hydrogen bonds in Figure 6b are hydrogen bonds between 25HBA molecules). This type of hydrogen bond interaction is strong, rigid, and difficult to extend or shorten considerably, and thus limits the crystal's a-axis change after heating [32–34]. In contrast, in the direction of the c-axis, TMP molecules are stacked by C-H···π interaction, which is weaker than hydrogen bonds and easier to change the molecular distance when the temperature changes.

The thermal expansion coefficients were calculated using the Pascal program [35] and the results were listed in Table 1. It demonstrates that, between 110 °C and 210 °C, the crystal exhibits predominantly negative thermal expansion in the direction of X_1 [−0.9994, 0.0000, −0.0349] with a coefficient value of −19.0021 MK^{-1} and predominantly positive thermal expansion in the directions of X_2 [0.0000, 1.0000, 0.0000] and X_3 [0.2691, 0.0000, 0.9631] with expansion coefficients of 7.3277 MK^{-1} and 82.9283 MK^{-1}. The anisotropic expansion/contraction of this unit cell is considered as the reason for crystal jumping.
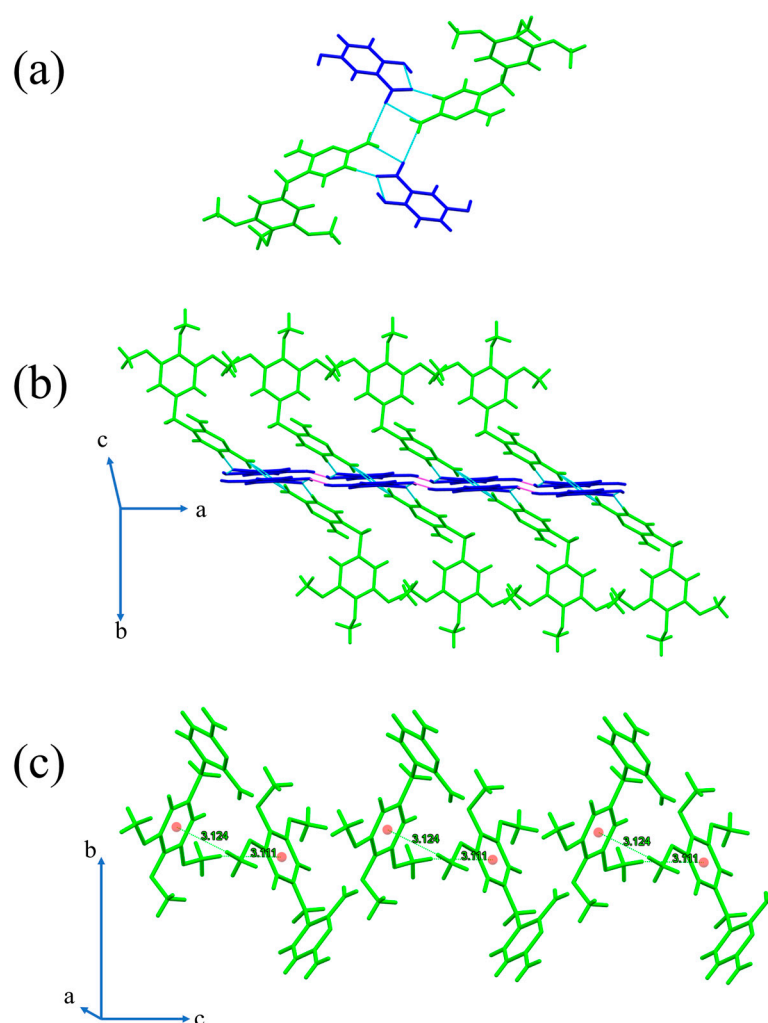
Figure 6. (**a**) The hetero-tetramer of TMP-25HBA. (**b**) A long chain of molecules formed by tetramers along the a-axis. (**c**) C-H⋯π stacking mode between TMP molecules along the c-axis.

Table 1. Calculated thermal expansion coefficients for TMP-25HBA.

			Direction		
Axes	α (MK^{-1})	σ_α (MK^{-1})	a	b	c
X_1	−19.0021	1.0841	−0.9994	0.0000	−0.0349
X_2	7.3277	0.1673	0.0000	1.0000	0.0000
X_3	82.9283	1.4665	0.2691	0.0000	0.9631
V	71.4168	1.5963			

Unit cell parameters of TMP-OA at high temperature were obtained by Rietveld refinement for VT-PXRD. Similarly, for TMP-OA, the temperature-dependent unit cell parameters (Figure 7a–c), the expansivity indicatrices (Figure 7d), and the calculated thermal expansion coefficients (Table 2) were analyzed. There were obvious differences in the lengths of the a and b axes of TMP-OA before and after the phase transition, especially at temperatures between 240 °C and 255 °C. During the heating process from 175 °C to 265 °C, the length of the a-axis increased by 2.3%, and the length of the b-axis decreased by 1.2%. Conversely, along the c-axis, the change in the length of c is relatively small.
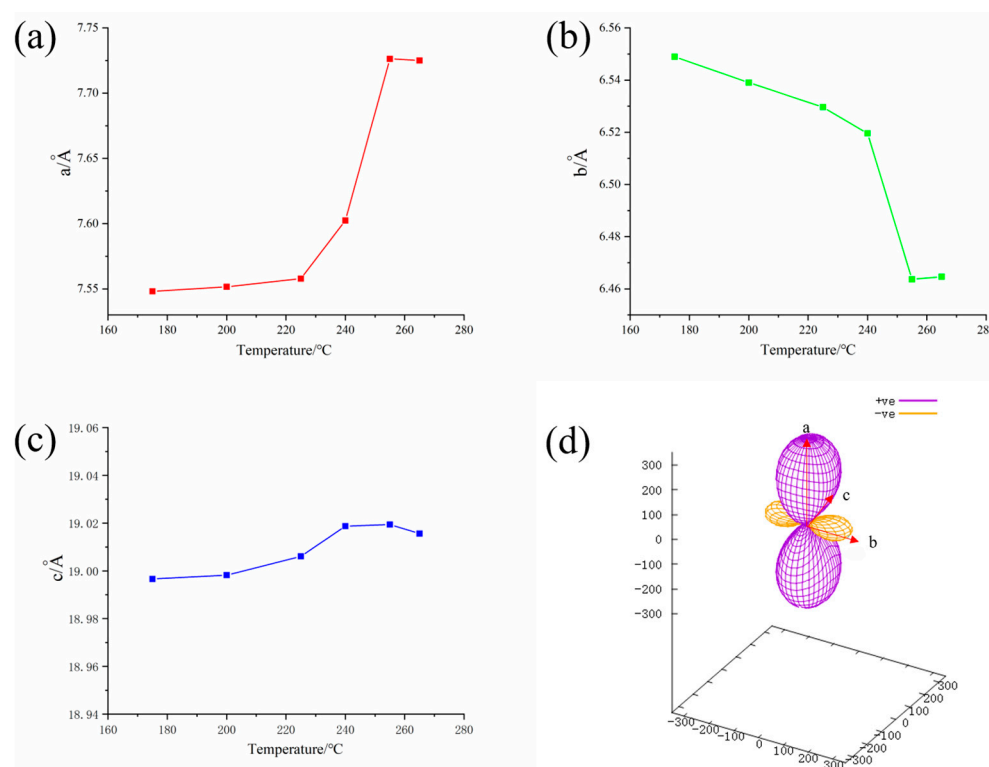
Figure 7. Temperature-dependent crystallographic parameters a (**a**), b (**b**) and c (**c**) axes and the expansivity indicatrices (**d**) of TMP-OA; purple and yellow represent positive and negative thermal expansion, respectively.

Table 2. Calculated thermal expansion coefficients for TMP-OA.

Axes	α (MK^{-1})	σ_α (MK^{-1})	Direction		
			a	b	c
X_1	-168.6973	19.7555	-0.2108	0.9757	-0.0596
X_2	35.3957	7.1966	0.4194	0.5539	0.7192
X_3	334.5309	52.3126	-0.8506	-0.5225	0.0585
V	243.9352	42.2856			

The calculated thermal expansion coefficients (Table 2) show negative thermal expansion mainly in the direction of X_1 [-0.2108, 0.9757, -0.0596] with the coefficient value of -168.6973 MK^{-1}, while the positive thermal expansion mainly occurs in the direction of X_3 [-0.8506, -0.5225, 0.0585] with the expansion coefficients of 334.5309 MK^{-1}. This anisotropic expansion was caused by phase transition and triggered the TS effect.

3.5. Molecular Conformation and Packing Comparison

In the asymmetric unit of the TMP-25HBA crystal, one molecule of TMP and one molecule of 25HBA are present, which form a cyclic motif of $R_2^2 8$. In order to reveal the mechanism of crystal jumping at the molecular level, the conformation of the asymmetric unit was analyzed.

When the temperature of the crystal was increased from 113 K to 463 K, the length of the two hydrogen bonds involving the $R_2^2 8$ motif changed, and the bond angle decreased. Specifically, the bond length of N_4-$H_{4B}\cdots O_7$ increased from 2.900 Å to 2.912 Å, and the bond angle decreased from 158.31° to 157.18°. Similarly, the bond length of N_3-$H_3\cdots O_6$ decreased from 2.668 Å to 2.661 Å, and the bond angle decreased from 178.34° to 177.24°. Furthermore, the angle between the benzene ring of 25HBA and the benzene ring of TMP increased from 35.28° to 39.08°, while the angle between the benzene and pyrimidine rings in TMP increased from 81.48° to 83.00°.

The conformational changes of asymmetric units were analyzed by overlaying O_1-O_2-O_3 atoms in the crystal structure at both high and low temperatures. Figure 8a–c shows that the conformation of asymmetric units has obviously changed, with the pyrimidine ring of TMP shifting by 0.313 Å, and the benzene ring of 25HBA shifting by 0.590 Å, in which the position of 25HBA connected by weaker interaction changed more significantly. The space occupied by asymmetric unit conformation decreases along the a-axis, and increases along the b and c axes, which is consistent with the change of unit cell axis with temperature. Therefore, it can be concluded that the conformation change of the asymmetric unit is the direct reason for the change of unit cell axis length. In addition, Figure 8d shows that the molecular packing of the crystal also changes slightly due to the change in the conformation of the asymmetric unit, manifesting as the slight deviation of the molecular position rather than the change in the overall molecular packing.
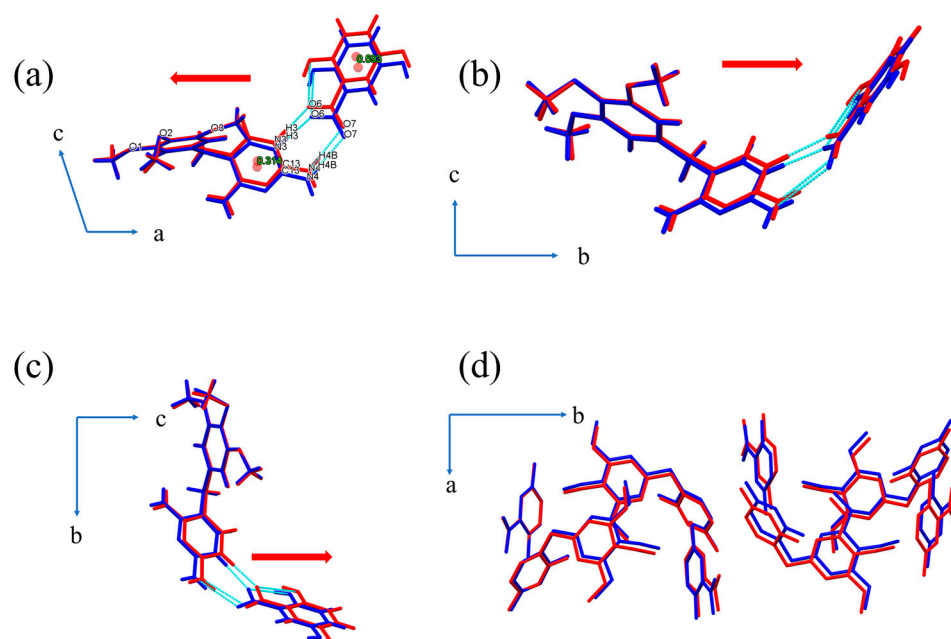

Figure 8. Conformations of the asymmetric unit at high and low temperature along different directions (**a–c**); (**d**) comparison of molecular packing at high and low temperature. (Blue is for low temperature and red is for high temperature).

Figure 9 presents the Hirshfeld surface analysis [36,37] of the two molecules in the TMP-25HBA crystal at different temperatures. It shows that the proportions of various intermolecular contacts do not change much. Therefore, further analysis of the energy frameworks [38] (Figure 10) was performed at the B3LYP/6-31G(d,p) level of theory. For each molecule (TMP and 25HBA), the interaction energy with the surrounding molecules within a radius of 3.8 Å was calculated.
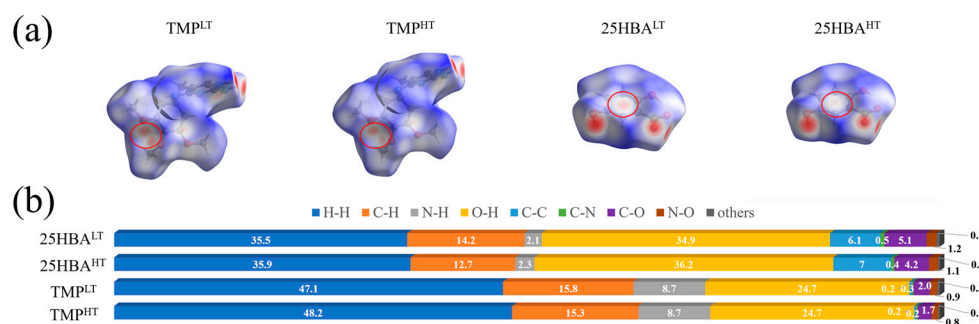

Figure 9. (**a**) 3D Hirshfeld surface of TMP and 25HBA at high/low temperatures; (**b**) percentage contributions of various intermolecular contacts to the Hirshfeld surface area.
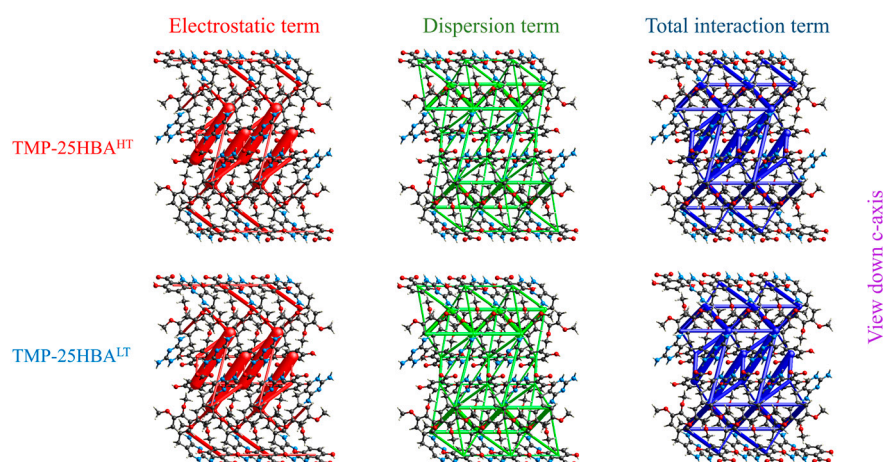
Figure 10. Energy frameworks corresponding to the different energy components and total interaction energy in TMP-25HBA^{LT} and TMP-25HBA^{HT}. The energy scaling factor is 88 and the energy threshold is 11 kJ/mol.

The total interaction energy (the average of the energies of the two molecules) is -308.1 kJ/mol in the TMP-25HBA^{LT}, including -204.8 kJ/mol of electrostatic, -123.4 kJ/mol of polarization, -262.0 kJ/mol of dispersion, and 267.4 kJ/mol of repulsive energy terms. For TMP-25HBA^{HT}, the total interaction energy (-302.0 kJ/mol) is composed of electrostatic (-188.0 kJ/mol), polarization (-117.6 kJ/mol), dispersion (-238.7 kJ/mol), and repulsive (223.4 kJ/mol) energy terms. The molecular interaction energies were calculated and shown in Figure S5 with scale factors of $k_{ele} = 1.019$, $k_{pol} = 0.651$, $k_{disp} = 0.901$, $k_{rep} = 0.811$. The total interaction energy of high temperature (-302.0 kJ/mol) conformation is smaller than that of low temperature conformation (-308.1 kJ/mol), indicating that the interaction between molecules weakens after the temperature rises. However, the interaction energy (Figure S5) between asymmetric units increased from -73.0 kJ/mol (high temperature) to -76.2 kJ/mol (low temperature), suggesting that asymmetric units have stronger interaction at high temperature. The interaction between molecules constituting asymmetric units is enhanced, but the interaction between these molecules and their surrounding molecules is weakened, which may lead to the anisotropic expansion/contraction of the whole unit cell. Energies between molecular pairs are represented as cylinders joining the centroids of pairs of molecules with the cylinder radius proportional to the relative strength of the corresponding interaction energy. It can also be seen from the energy frameworks that the radius of the cylinder between asymmetric units is the largest, contributing the most to the structure. The design of such temperature-sensitive supramolecular structure may provide a new way to discover TS crystals.

Based on the analysis, the TS effect of TMP-25HBA and TMP-OA can be explained. TMP was combined with 25HBA by hydrogen bonding to form a twisted angle between aromatic rings. The change of dihedral angle between aromatic rings and the shift of centroid of aromatic rings in asymmetric cells after temperature rise lead to anisotropic expansion/contraction of the cell and further crystal jumping. Although the conformational change is not very significant, the sudden release of structural stress may be sufficient to cause the TS effect [17]. For systems that do not undergo phase transition, there is still no very precise and all-around understanding of the TS effect. Although the energy framework is useful for this work, it cannot fully explain crystal jumping. For jumping crystals, we still need to conduct more in-depth research.

Because the phase transition temperature of TMP-OA is higher than the upper limit of our single crystal diffractometer equipment, the single crystal structure of TMP-OA at high temperature is not obtained. Nevertheless, the anisotropic expansion of the unit cell caused by phase transition can be considered as the reason for the jump of the TMP-OA crystal.

4. Conclusions

This work investigated the development of two types of multicomponent TS crystals, achieved by combining two molecules into distorted conformations via weak intermolecular interactions. It was observed that TMP-25HBA did not undergo a phase transition, but changes in its conformation and intermolecular interactions may induce structural strains and trigger the TS effect. On the other hand, TMP-OA underwent a phase transition. The phase transition was validated through DSC and VT-PXRD techniques. Rietveld refinement for VT-PXRD confirmed that the TS effect was triggered by anisotropic expansion. This suggests that the formation of a twisted angle between aromatic rings may help design TS crystals. The co-crystallization technique used in crystal engineering can provide inspiration for this concept's design. We believe that the design of TS crystals will no longer be a mystery as we are currently working on additional attempts at designing twisted conformations.

Supplementary Materials: The following supporting information can be downloaded at: https://www.mdpi.com/article/10.3390/cryst13040701/s1 and https://zenodo.org/record/7698506#.ZBR9qRRBy4Q (accessed on 3 March 2023). Movie S1: Heating of TMP-25HBA starting at 180 °C (heating rate 10 K/min); Movie S2: Heating of TM-OA in cycle 1 starting at 250 °C (heating rate 10 K/min).; Movie S3: Cooling of TMP-OA in cycle 1 starting at 234 °C (cooling rate 10 K/min); Movie S4: Heating of TM-OA in cycle 2 starting at 248 °C (heating rate 10 K/min).; Movie S5: Cooling of TMP-OA in cycle 2 starting at 238 °C (cooling rate 10 K/min). Figure S1. Molecular structural formulas of thermosalient crystals without phase transitions that have been previously reported. Figure S2. (a) Differential scanning calorimetry thermograms of two cycles of TMP-25HBA powder. (b) Differential scanning calorimetry thermograms of two cycles of TMP-OA powder. Figure S3. (a) Tetramer of TMP with 25HBA; (b) 1 D chain formed by tetramers; (c) 2 D plane connected by 1 D chains (green and yellow) (d) 3 D structure arranged between 2 D planes. Figure S4. (a) Tetramer formed between TMP and OA; (b) 1 D chain of Tetramers; (c) The plane connected between the chains; (d) Connection mode of TMP-OA between planes. Figure S5. 2D fingerprints of different molecules in TMP-25HBA crystals (HT is high temperature, LT is low temperature). Figure S6. (a) and (b) are the energy calculation results of TMP in TMP-25HBALT; (e,f) are the energy calculation results of 25HBA in TMP-25HBALT; (c,d) are the energy calculation results of TMP in TMP-25HBAHT; (g,h) are the energy calculation results of 25HBA in TMP-25HBAHT. Figure S7. The melting point of the crystal was determined by HSM (To prevent the crystal from jumping out of sight, the crystal was covered with a glass sheet.) and the T(TS)/T(melting) was calculated. T(TS)/T(melting) of TMP-25HBA is 456.15K/513.15K (0.8889). T(TS)/T(melting) of TMP-OA is 533.15K/553.15K (0.9638). Table S1. Crystallographic Parameters of TMP-25HBA and TMP-OA. Table S2. Cell parameters of TMP-25HBA at different temperatures. Table S3. Cell parameters of TMP-OA at different temperatures.

Author Contributions: Writing—original draft preparation, X.H.; writing—review and editing, C.X.; conceptualization, X.H., L.Q. and Y.B.; methodology, X.H. and Y.X.; software, X.H. and Y.Y.; validation, Y.S. All authors have read and agreed to the published version of the manuscript.

Data Availability Statement: The data presented in this study are available on request from the corresponding author.

Conflicts of Interest: The authors declare no conflict of interest.

References

1. Naumov, P.; Karothu, D.P.; Ahmed, E.; Catalano, L.; Commins, P.; Mahmoud Halabi, J.; Al-Handawi, M.B.; Li, L. The Rise of the Dynamic Crystals. *J. Am. Chem. Soc.* **2020**, *142*, 13256–13272. [CrossRef]
2. Karamertzanis, P.G.; Price, S.L. Energy Minimization of Crystal Structures Containing Flexible Molecules. *J. Chem. Theory Comput.* **2006**, *2*, 1184–1199. [CrossRef]
3. Rath, B.B.; Vittal, J.J. Photoreactive Crystals Exhibiting [2 + 2] Photocycloaddition Reaction and Dynamic Effects. *Acc. Chem. Res.* **2022**, *55*, 1445–1455. [CrossRef] [PubMed]

4. Abendroth, J.M.; Bushuyev, O.S.; Weiss, P.S.; Barrett, C.J. Controlling Motion at the Nanoscale: Rise of the Molecular Machines. *ACS Nano* **2015**, *9*, 7746–7768. [CrossRef] [PubMed]

5. Li, L.; Commins, P.; Al-Handawi, M.B.; Karothu, D.P.; Halabi, J.M.; Schramm, S.; Weston, J.; Rezgui, R.; Naumov, P. Martensitic Organic Crystals as Soft Actuators. *Chem. Sci.* **2019**, *10*, 7327–7332. [CrossRef] [PubMed]

6. Dong, Y.; Wang, J.; Guo, X.; Yang, S.; Ozen, M.O.; Chen, P.; Liu, X.; Du, W.; Xiao, F.; Demirci, U.; et al. Multi-Stimuli-Responsive Programmable Biomimetic Actuator. *Nat Commun* **2019**, *10*, 4087. [CrossRef]

7. Dattler, D.; Fuks, G.; Heiser, J.; Moulin, E.; Perrot, A.; Yao, X.; Giuseppone, N. Design of Collective Motions from Synthetic Molecular Switches, Rotors, and Motors. *Chem. Rev.* **2020**, *120*, 310–433. [CrossRef]

8. Naumov, P.; Chizhik, S.; Panda, M.K.; Nath, N.K.; Boldyreva, E. Mechanically Responsive Molecular Crystals. *Chem. Rev.* **2015**, *115*, 12440–12490. [CrossRef]

9. Desta, I.T.; Chizhik, S.A.; Sidelnikov, A.A.; Karothu, D.P.; Boldyreva, E.V.; Naumov, P. Mechanically Responsive Crystals: Analysis of Macroscopic Strain Reveals "Hidden" Processes. *J. Phys. Chem. A* **2020**, *124*, 300–310. [CrossRef]

10. Karothu, D.P.; Mahmoud Halabi, J.; Li, L.; Colin-Molina, A.; Rodríguez-Molina, B.; Naumov, P. Global Performance Indices for Dynamic Crystals as Organic Thermal Actuators. *Adv. Mater.* **2020**, *32*, 1906216. [CrossRef]

11. Hean, D.; Alde, L.G.; Wolf, M.O. Photosalient and Thermosalient Crystalline Hemithioindigo-Anthracene Based Isomeric Photoswitches. *J. Mater. Chem. C* **2021**, *9*, 6789–6795. [CrossRef]

12. Duan, Y.; Semin, S.; Tinnemans, P.; Xu, J.; Rasing, T. Fully Controllable Structural Phase Transition in Thermomechanical Molecular Crystals with a Very Small Thermal Hysteresis. *Small* **2021**, *17*, 2006757. [CrossRef] [PubMed]

13. Hagiwara, H.; Konomura, S. Thermosalience Coupled to Abrupt Spin Crossover with Dynamic Ligand Motion in an Iron(II) Molecular Crystal. *CrystEngComm* **2022**, *24*, 4224–4234. [CrossRef]

14. Takazawa, K.; Inoue, J.; Matsushita, Y. Repeatable Actuations of Organic Single Crystal Fibers Driven by Thermosalient-Phase-Transition-Induced Buckling. *Small* **2022**, *18*, 2204500. [CrossRef] [PubMed]

15. Chen, Y.; Jing, B.; Chang, Z.; Gong, J. Desolvation Induced Crystal Jumping: Reversible Hydration and Dehydration of a Spironolactone–Saccharin Cocrystal with Water as the Jumping-Mate. *CrystEngComm* **2021**, *23*, 6838–6842. [CrossRef]

16. Sahoo, S.C.; Panda, M.K.; Nath, N.K.; Naumov, P. Biomimetic Crystalline Actuators: Structure–Kinematic Aspects of the Self-Actuation and Motility of Thermosalient Crystals. *J. Am. Chem. Soc.* **2013**, *135*, 12241–12251. [CrossRef]

17. Klaser, T.; Popović, J.; Fernandes, J.; Tarantino, S.; Zema, M.; Skoko, Ž. Does Thermosalient Effect Have to Concur with a Polymorphic Phase Transition? The Case of Methscopolamine Bromide. *Crystals* **2018**, *8*, 301. [CrossRef]

18. Colin-Molina, A.; Karothu, D.P.; Jellen, M.J.; Toscano, R.A.; Garcia-Garibay, M.A.; Naumov, P.; Rodríguez-Molina, B. Thermosalient Amphidynamic Molecular Machines: Motion at the Molecular and Macroscopic Scales. *Matter* **2019**, *1*, 1033–1046. [CrossRef]

19. Seki, T.; Mashimo, T.; Ito, H. Anisotropic Strain Release in a Thermosalient Crystal: Correlation between the Microscopic Orientation of Molecular Rearrangements and the Macroscopic Mechanical Motion. *Chem. Sci.* **2019**, *10*, 4185–4191. [CrossRef]

20. Tamboli, M.I.; Karothu, D.P.; Shashidhar, M.S.; Gonnade, R.G.; Naumov, P. Effect of Crystal Packing on the Thermosalient Effect of the Pincer-Type Diester Naphthalene-2,3-Diyl-Bis(4-Fluorobenzoate): A New Class II Thermosalient Solid. *Chem. Eur. J.* **2018**, *24*, 4133–4139. [CrossRef]

21. Sahoo, S.C.; Sinha, S.B.; Kiran, M.S.R.N.; Ramamurty, U.; Dericioglu, A.F.; Reddy, C.M.; Naumov, P. Kinematic and Mechanical Profile of the Self-Actuation of Thermosalient Crystal Twins of 1,2,4,5-Tetrabromobenzene: A Molecular Crystalline Analogue of a Bimetallic Strip. *J. Am. Chem. Soc.* **2013**, *135*, 13843–13850. [CrossRef] [PubMed]

22. Skoko, Ž.; Zamir, S.; Naumov, P.; Bernstein, J. The Thermosalient Phenomenon. "Jumping Crystals" and Crystal Chemistry of the Anticholinergic Agent Oxitropium Bromide. *J. Am. Chem. Soc.* **2010**, *132*, 14191–14202. [CrossRef] [PubMed]

23. Takeda, T.; Ozawa, M.; Akutagawa, T. Jumping Crystal of a Hydrogen-Bonded Organic Framework Induced by the Collective Molecular Motion of a Twisted π System. *Angew. Chem. Int. Ed.* **2019**, *58*, 10345–10352. [CrossRef] [PubMed]

24. Shibuya, Y.; Itoh, Y.; Aida, T. Jumping Crystals of Pyrene Tweezers: Crystal-to-Crystal Transition Involving π / π -to-CH/ π Assembly Mode Switching. *Chem. Asian J.* **2017**, *12*, 811–815. [CrossRef] [PubMed]

25. Jin, M.; Yamamoto, S.; Seki, T.; Ito, H.; Garcia-Garibay, M.A. Anisotropic Thermal Expansion as the Source of Macroscopic and Molecular Scale Motion in Phosphorescent Amphidynamic Crystals. *Angew. Chem. Int. Ed.* **2019**, *58*, 18003–18010. [CrossRef] [PubMed]

26. Seki, T.; Mashimo, T.; Ito, H. Crystal Jumping of Simple Hydrocarbons: Cooling-Induced Salient Effect of Bis-, Tri-, and Tetraphenylethene through Anisotropic Lattice Dimension Changes without Thermal Phase Transitions. *Chem. Lett.* **2020**, *49*, 174–177. [CrossRef]

27. Kato, K.; Seki, T.; Ito, H. (9-Isocyanoanthracene)Gold(I) Complexes Exhibiting Two Modes of Crystal Jumps by Different Structure Change Mechanisms. *Inorg. Chem.* **2021**, *60*, 10849–10856. [CrossRef]

28. Miura, Y.; Takeda, T.; Yoshioka, N.; Akutagawa, T. Thermosalient Effect of 5-Fluorobenzoyl-4-(4-Methoxyphenyl)Ethynyl-1-Methylimidazole without Phase Transition. *Crystal Growth Design* **2022**, *22*, 5904–5911. [CrossRef]

29. Spackman, P.R.; Turner, M.J.; McKinnon, J.J.; Wolff, S.K.; Grimwood, D.J.; Jayatilaka, D.; Spackman, M.A. *CrystalExplorer*: A Program for Hirshfeld Surface Analysis, Visualization and Quantitative Analysis of Molecular Crystals. *J. Appl. Crystallogr.* **2021**, *54*, 1006–1011. [CrossRef]

30. Omoto, K.; Nakae, T.; Nishio, M.; Yamanoi, Y.; Kasai, H.; Nishibori, E.; Mashimo, T.; Seki, T.; Ito, H.; Nakamura, K.; et al. Thermosalience in Macrocycle-Based Soft Crystals via Anisotropic Deformation of Disilanyl Architecture. *J. Am. Chem. Soc.* **2020**, *142*, 12651–12657. [CrossRef]

31. Rath, B.B.; Gallo, G.; Dinnebier, R.E.; Vittal, J.J. Reversible Thermosalience in a One-Dimensional Coordination Polymer Preceded by Anisotropic Thermal Expansion and the Shape Memory Effect. *J. Am. Chem. Soc.* **2021**, *143*, 2088–2096. [CrossRef] [PubMed]

32. Decremps, F.; Fischer, M.; Polian, A.; Itié, J.P.; Sieskind, M. Ionic Layered PbFCl-Type Compounds under High Pressure. *Phys. Rev. B* **1999**, *59*, 4011–4022. [CrossRef]

33. Ardit, M.; Cruciani, G.; Dondi, M.; Garbarino, G.L.; Nestola, F. Phase Transitions during Compression of Thaumasite, $Ca_3Si(OH)_6(CO_3)(SO_4) \cdot 12H_2O$: A High-Pressure Synchrotron Powder X-Ray Diffraction Study. *Mineral. Mag.* **2014**, *78*, 1193–1208. [CrossRef]

34. Arkhipov, S.G.; Losev, E.A.; Nguyen, T.T.; Rychkov, D.A.; Boldyreva, E.V. A Large Anisotropic Plasticity of L -Leucinium Hydrogen Maleate Preserved at Cryogenic Temperatures. *Acta Crystallogr. B Struct. Sci. Cryst. Eng. Mater.* **2019**, *75*, 143–151. [CrossRef] [PubMed]

35. Cliffe, M.J.; Goodwin, A.L. *PASCal*: A Principal Axis Strain Calculator for Thermal Expansion and Compressibility Determination. *J. Appl. Crystallogr.* **2012**, *45*, 1321–1329. [CrossRef]

36. Spackman, M.A.; Jayatilaka, D. Hirshfeld Surface Analysis. *CrystEngComm* **2009**, *11*, 19–32. [CrossRef]

37. McKinnon, J.J.; Mitchell, A.S.; Spackman, M.A. Hirshfeld Surfaces: A New Tool for Visualising and Exploring Molecular Crystals. *Chem. Eur. J.* **1998**, *4*, 2136–2141. [CrossRef]

38. Mackenzie, C.F.; Spackman, P.R.; Jayatilaka, D.; Spackman, M.A. *CrystalExplorer* Model Energies and Energy Frameworks: Extension to Metal Coordination Compounds, Organic Salts, Solvates and Open-Shell Systems. *IUCrJ* **2017**, *4*, 575–587. [CrossRef]